ARMY RESEARCH LABORATORY

Comparison of the Inversion Periods for Mid-wave IR (MidIR) and Long-wave IR (LWIR) Polarimetric and Conventional Thermal Imagery

by M. Felton, K. P. Gurton, J. L. Pezzaniti, D. B. Chenault, and L. E. Roth

ARL-TR-5153 **April 2010**

NOTICES

Disclaimers

The findings in this report are not to be construed as an official Department of the Army position unless so designated by other authorized documents.

Citation of manufacturer's or trade names does not constitute an official endorsement or approval of the use thereof.

Destroy this report when it is no longer needed. Do not return it to the originator.

Army Research Laboratory
Adelphi, MD 20783-1197

ARL-TR-5153 **April 2010**

Comparison of the Inversion Periods for Mid-wave IR (MidIR) and Long-wave IR (LWIR) Polarimetric and Conventional Thermal Imagery

M. Felton and K. P. Gurton
Computational and Information Sciences Directorate, ARL

J. L. Pezzanitib and D. B. Chenault
Polaris Sensor Technologies, Inc.
200 Westside Square, Suite 320, Huntsville, AL, 35801

L. E. Roth
U.S. Army Armament Research and Development Engineering Center
Picatinny Arsenal, NJ, USA 07806-5000

REPORT DOCUMENTATION PAGE

Form Approved
OMB No. 0704-0188

1. REPORT DATE *(DD-MM-YYYY)*	2. REPORT TYPE	3. DATES COVERED (From - To)
April 2010	Summary	

4. TITLE AND SUBTITLE
Comparison of the Inversion Periods for Mid-wave IR (MidIR) and Long-wave IR (LWIR) Polarimetric and Conventional Thermal Imagery

5a. CONTRACT NUMBER

5b. GRANT NUMBER

5c. PROGRAM ELEMENT NUMBER

6. AUTHOR(S)
M. Felton, K. P. Gurton, J. L. Pezzaniti, D. B. Chenault, and L. E. Roth

5d. PROJECT NUMBER

5e. TASK NUMBER

5f. WORK UNIT NUMBER

7. PERFORMING ORGANIZATION NAME(S) AND ADDRESS(ES)
U.S. Army Research Laboratory
ATTN: RDRL-CIE-S
2800 Powder Mill Road
Adelphi, MD 20783-1197

8. PERFORMING ORGANIZATION REPORT NUMBER
ARL-TR-5153

9. SPONSORING/MONITORING AGENCY NAME(S) AND ADDRESS(ES)

10. SPONSOR/MONITOR'S ACRONYM(S)

11. SPONSOR/MONITOR'S REPORT NUMBER(S)

12. DISTRIBUTION/AVAILABILITY STATEMENT
Approved for public release; distribution unlimited.

13. SUPPLEMENTARY NOTES

14. ABSTRACT

We report the results of a diurnal study that recorded radiometrically calibrated polarimetric and conventional thermal imagery in the mid-wave IR (MidIR) and long-wave IR (LWIR) to identify and compare the respective time periods in which minimum target contrast is achieved. The MidIR polarimetric sensor is based on a division-of-aperture approach and has a 640×512 indium antimonide (InSb) focal-plane array (FPA), while the LWIR polarimetric sensor uses a spinning achromatic retarder to perform polarimetric filtering and has a 324 x 256 microbolometer FPA. The images used in this study include the S_0 and S_1 Stokes images of a scene containing a military vehicle and the natural background. Relevant meteorological parameters measured during the test period include air temperature, ambient loading in the LWIR, relative humidity, cloud cover, height, and density. The data show that the chief factors affecting polarimetric contrast in both wavebands are the amount of thermal emission from the objects in the scene and the abundance of MidIR and LWIR sources in the optical background. In particular, we observed that the MidIR polarimetric contrast was positively correlated to the presence of MidIR sources in the optical background, while the LWIR polarimetric contrast was negatively correlated to the presence of LWIR sources in the optical background.

15. SUBJECT TERMS
Polarimetric imaging, thermal imaging, microbolometer, target contrast, inversion periods

16. SECURITY CLASSIFICATION OF:			17. LIMITATION OF ABSTRACT	18. NUMBER OF PAGES	19a. NAME OF RESPONSIBLE PERSON
a. REPORT	b. ABSTRACT	c. THIS PAGE			M. Felton
Unclassified	Unclassified	Unclassified	UU	26	19b. TELEPHONE NUMBER (*Include area code*) (301) 394-2618

Standard Form 298 (Rev. 8/98)
Prescribed by ANSI Std. Z39.18

Contents

List of Figures

List of Tables

Acknowledgments

This work was accomplished using data from the Hyperspectral and Polarimetric Target Detection Program at the Precision Armament Laboratory (PAL) Tower at the Armament Research and Development Engineering Center (ARDEC) with the help of Mr. Joao Romano (Program Manager), Mr. Mark Woolley (PAL Manager), and Zed Habte (test engineer).

INTENTIONALLY LEFT BLANK.

1. Introduction

Thermal imagers have been established as the primary tool used in military and security activities that involve surveillance, targeting and tracking, and night-time operations. Unlike image intensification (I^2) devices, which depend on ambient light levels, thermal imagers exploit the fact that all objects with a temperature above 0 K emit thermal radiation by creating a pseudo-image of the scene based on this thermal emission. The two thermal imaging windows are the mid-wave IR (MidIR), 3–5 μm, and the long-wave IR (LWIR), 8–14 μm, both chosen for the relatively low amounts of absorption from atmospheric species, such as carbon dioxide (CO_2) and water (H_2O).

Contrast between the objects within a thermal image is determined by their effective temperatures, which are a function of their true temperature and emissivity, a characteristic that describes how efficiently an object radiates absorbed energy as compared to a blackbody. If there is no thermal contrast between a target and its background, it cannot be seen in a thermal image. The diurnal cycles of the thermal properties of both manmade and natural objects tend to bring about periods of low contrast within thermal images, often referred to as thermal crossovers or inversion periods (*1*). These inversion periods tend to occur during periods of rapidly changing temperatures, such as sunrise and sunset, but may occur at any time throughout the day, depending both on temperature differences between objects and their backgrounds, and on environmental factors, such as solar loading. Thermal polarimetric imaging is a technology that enhances conventional thermal imaging by extending its operational ability into these periods of thermal inversion.

1.1 Thermal Polarimetric Imaging

Thermal polarimetric imaging has been proposed as a method to enhance conventional thermal imaging (*2*). It creates images of a scene that are based on the states of polarization of the IR light emitted or reflected from the objects within the scene. An object's polarimetric signature is a function of its surface geometry and roughness. Due to the different geometrical and roughness features of objects constituting natural backgrounds and manmade objects, the polarization states of the emitted and reflected thermal light can be used as a discriminator between objects of interest and background clutter. Using the polarization of the light, it is possible to obtain an image of a scene that has polarimetric contrast between objects and their backgrounds even when there is no thermal contrast.

In addition to the environmental factors that affect thermal contrast, there are also environmental factors that affect polarimetric contrast. The most significant of these factors involves sources of IR radiation in what has been referred to as the optical background. The optical background is defined as the IR radiation emitted by sources that are not necessarily visible within the scene,

but that still reflects off of an object and into the field of view (FOV) of the camera (*3*). Potential sources include vehicles, buildings, trees, clouds, water vapor, etc. The optical background can become partially polarized upon reflection and act as a competing component to the emitted polarized light. Polarized emitted and reflected light are often orthogonal to each other, because the emitted polarized light tends to be in the direction parallel to the surface normal, while light polarized upon reflection tends to be perpendicular to the surface normal. When the two components superpose, the effect can be a reduction in the magnitude of the polarimetric signature of an object.

This study compares the temporal occurrence of conventional thermal inversion periods to polarimetric inversion periods and correlates these inversions with environmental factors. Our goals are to quantify the periods of time in which contrast within polarimetric images is present while conventional thermal contrast has been lost and to verify the impact of environmental factors such as clouds. Under these conditions, it can be concluded that polarimetric imaging is capable of enhancing conventional thermal imaging.

2. Experiment

2.1 MidIR Polarimetric Sensor

A schematic of a division-of-aperture (DOA) MidIR imaging polarimeter architecture is illustrated in figure 1. A picture of the actual system is shown in figure 2. The system is based on a DOA lens technology developed by Polaris Sensor Technologies (*4*). The first element of the lens system (in figure 1) is a standard MidIR objective lens, which forms an image of the target on a field stop. The second set of optics shown inside the cryogenic chamber is the DOA optics. The collimation optic collimates the image from the field stop and forms an image of the objective lens aperture onto a 2×2 array of mini-lenses. The mini-lenses are in quasi-collimated space. The mini-lens set forms four identical images of the field stop onto four quadrants of the sensor focal plane array (FPA). When the DOA system operates as an imaging polarimeter, each mini-lens is followed by a linear polarizer at a different orientation. The DOA system can also be operated as a multi-spectral imager if each mini-lens is followed by a bandpass filter. For this system, a set of four linear wire-grid polarizers is used, oriented at angles 0°, 90°, 45°, and 135°. Thus, the FPA captures four images simultaneously of the object at these four different polarization states. The four images are precisely registered to within 1/10 pixel in software, and weighted subtractions are done to compute the Stokes images of the scene. The actual DOA lens set is much more complex than the schematic shown here and involves nine elements, but this illustrates the concept. Note that the image shown in figure 1 is an actual image taken with the system from the air of the Saturn V rocket located at the Space and Rocket Center, Huntsville, AL. The DOA output image shown to the right in figure 1 is actual output from the DOA lens set. Table 1 gives the optical specifications for the DOA MidIR imaging polarimeter.

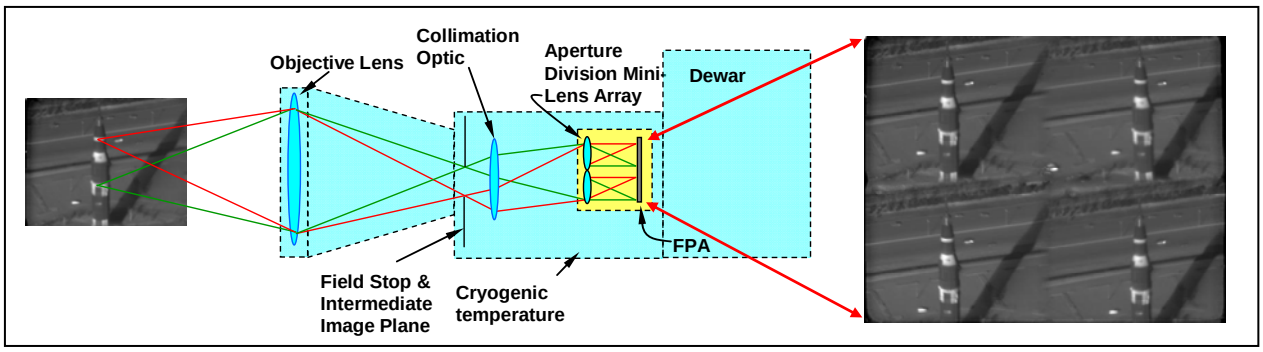

Figure 1. Schematic of the U.S. Army Research Laboratory (ARL) MidIR DOA imaging polarimeter.

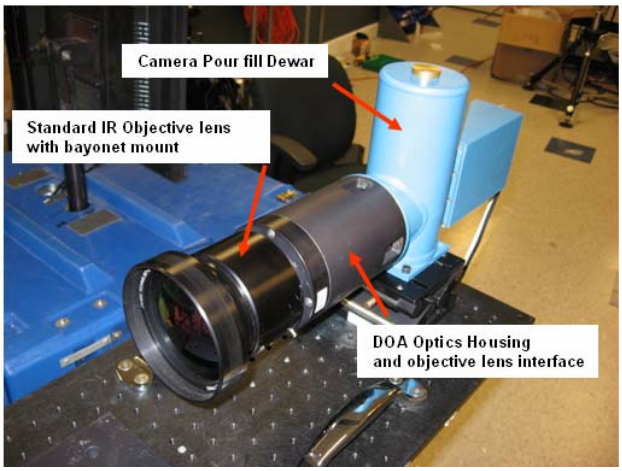

Figure 2. ARL MidIR imaging polarimeter with DOA optics.

Table 1. A summary of the MidIR sensor optical specs.

Parameter	Value
FOV	5.5°
Objective focal length	100 mm
f/#	2.3
Total FPA pixels	640×512
Pixel size	24×24 µm
Quadrant aperture usable pixels	220×220
Max frame rate (stream to disk)	87 fps (640×512)
Sensor dimensions (mm)	420L×90W×210H
Sensor weight	11 lb
System noise equivalent radiance (NER)	1e-7 W/cm^2-sr

2.2 LWIR Polarimetric Sensor

The LWIR imaging polarimeter is a microbolometer-based rotating retarder imaging polarimeter developed by Polaris Sensor Technologies, Inc., Huntsville, AL (figure 3) (5). It operates by capturing up to 12 images sequentially in time, each at a different orientation of the rotating retarder. Together, the retarder and linear polarizer act as a polarization state analyzer for the

light forming the image. Using the data reduction matrix method, the Stokes vectors are calculated, which completely characterizes the polarization states of the light from the scene. Table 2 lists the sensor specifications.

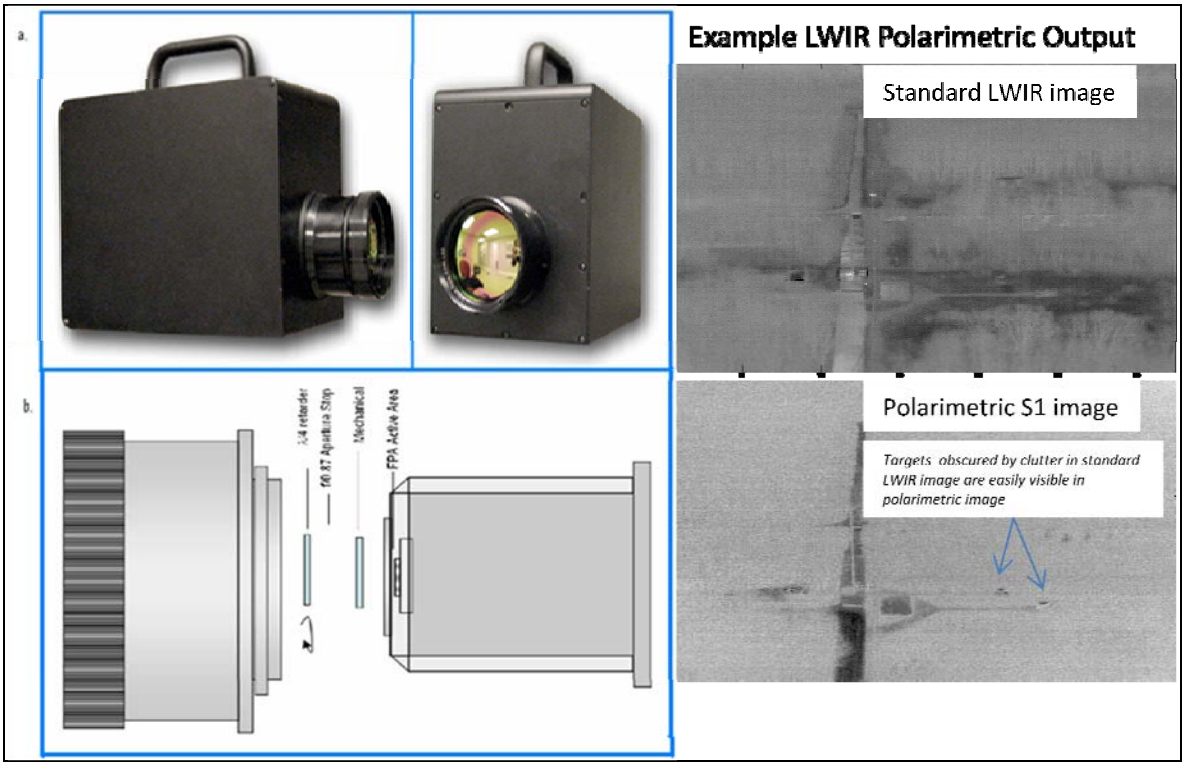

Figure 3. (Left) Picture of polarimetric sensor, and optical layout of the spinning retarder, microbolometer-based sensor, and (right) standard and polarimetric LWIR images. Note how background clutter in standard LWIR image is rejected in polarimetric image, revealing targets difficult to see in LWIR image.

Table 2. Specifications for the LWIR imaging polarimeter.

Parameter	Value
FOV	13.7°×11.0°
Objective focal length	50 mm
f/#	0.87
Total FPA pixels	324×256
Pixel size	38×38 μm
Max frame rate (stream to disk)	30 fps
Sensor dimensions (mm)	10L × 6W × 7.5H
Sensor weight	12 lb
Power	15 V, 1.2 A

2.3 Field Test Site

The test was conducted at the Precision Armaments Laboratory located in Picatinny Arsenal, NJ. The camera was situated on the sixth floor of a tower (approximately 200 ft high) looking out of the windows towards the target site, which was at ~0.5 km in range and consisted of two military

vehicles and natural backgrounds, including grass, brush, and trees (figures 4 and 5). In addition to the 200-ft elevation of the sixth floor of the tower, the tower, itself, was situated on top of a ridge ~175 ft above the target site.

Figure 4. Precision Armaments Laboratory tower with elevator that housed the polarimetric sensor situated on the sixth floor.

Figure 5. Target site consisting of two military vehicles and a natural background. The test was conducted on May 13, 2009, but this image was taken in the preceding fall. Therefore, during the test, the grass was alive and thick, and the bushes and trees contained leaves.

Environmental measurements available at the target site include air temperature, relative humidity, ceilometer data, and pyrgeometer (precision infrared radiometer [PIR]) data. The ceilometer provides real-time reports of cloud bases and depths directly above the ceilometer, and determines cloud cover by using a weighted average of 30-s cloud hit reports over a 30-min period. The pyrgeometer measured ambient LWIR radiation from 3–50 μm within a 2π steradian FOV.

The data acquisition clocks for the environmental data and the camera were synced to ensure coincident data. The temporal resolutions of the data are as follows: air temperature, relative humidity and pyrgeometer—2 s; ceilometer—10 s; and camera—10 min. Data were acquired continuously between 00:00 and 23:00 on May 13, 2009.

2.4 Image Analysis

A contrast-based study was performed between the military vehicles and their immediate backgrounds. A contrast-based study was also performed between a target (surrogate tank) and its immediate backgrounds. Data for the target directly facing the tower in figure 5 is used in the analysis. The exact scene used in the analysis is shown in figure 6 and consists of the surrogate tank and the surrounding grass and trees/brush. This target was selected because most of its surfaces are oriented in the same direction relative to the FOV of the camera. Therefore, widely varying magnitudes of polarimetric signatures due to diversity of surface geometry minimally affect the target's mean signatures.

Figure 6. The test target and its natural background. The target, grass and trees regions of interest correspond to the blue, red and green boxes, respectively.

The data products used in this study include S_0 and S_1, where S_0 is the total intensity (equivalent to conventional thermal image), and S_1 is the horizontal minus the vertical components of polarization. The S_2 Stokes parameter (+45° minus –45° polarized components) and degree of linear polarization are excluded because the positive 45° quadrant of the MidIR sensor was not functioning properly, and so these data were not available for comparison with the corresponding LWIR parameters. Because S_0 and S_1 are of different magnitudes, the analysis was performed on standardized versions of these images (*6, 7*). Specifically, each image had its mean subtracted and was normalized by its standard deviation. This made it possible to directly compare the contrasts for both the S_0 and S_1 images. Using temporal sequences of co-registered images, regions of interest were defined for the target and its backgrounds, and the mean values were calculated for both data products at each time in the series. The contrast is defined as the absolute value of the difference between the mean target value, $\acute{\mu}_t$, and the mean background value, $\acute{\mu}_b$, where the prime indicates that the means were calculated using standardized images:

$$\text{contrast} = |\acute{\mu}_t - \acute{\mu}_b|. \quad (1)$$

Because standardizing the images gives them unitless values, the contrast defined by equation 1 is also unitless.

Examples of contrast values calculated using equation 1 and their corresponding images are shown in figure 7. The contrasts were calculated for the LWIR S_0 images of the scene in figure 6, taken at three different times of the day. Because this scene has two different natural backgrounds, one is chosen at a time to calculate the contrast between the target and the chosen background. In the case of figure 7, the grass background is used to calculate the contrast.

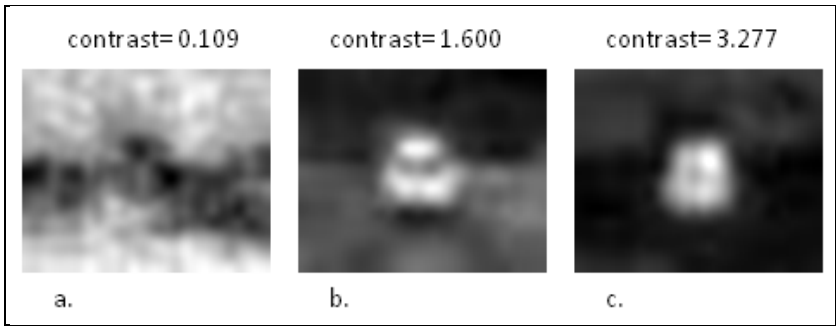

Figure 7. Example contrast values comparing the target to the grass and the corresponding S_0 image taken at a. 07:00, b. 11:00, and c. 19:00.

3. Results

The results are presented in the form of two different types of plots. The first is diurnal plots of standardized S_0 and S_1, which allow for a more direct comparison between the MidIR and LWIR data, as well as between S_0 and S_1 for each waveband. It must be remembered, though, that the standardized data are unitless. In general, S_0 magnitudes are greater than S_1 magnitudes because light from the scene must be filtered out in order to obtain the S_1 image. In addition, LWIR signatures are generally stronger than MidIR signatures due to the efficiency at which ambient objects emit in the LWIR as opposed to the MidIR. The second type of plot is diurnal contrast plots calculated using equation 1. Included with each of these plots are the corresponding environmental data. The ceilometer data are omitted because the cloud information can be obtained from the pyrgeometer (PIR) data. A direct comparison of ceilometer and pyrgeometer data revealed that the baseline reading for a cloudless daytime sky was roughly 275–280 W/m^2. Any value higher than this typically indicates the presence of clouds such that the higher the value, the thicker the cloud cover. During this study, sunrise and sunset occurred at roughly 05:00 and 20:00, respectively.

3.1 Diurnal Standardized S_0 and S_1

Figures 8 presents the MidIR and LWIR standardized diurnal plots of S_0 values for the regions of interest defined in figure 6 corresponding to the surrogate tank, grass, and trees. The missing MidIR data corresponds to periods in which non-uniformity corrections were performed. As expected, the S_0 values for the regions of interest mirror each other in both wavebands, although the use of standardized data masks the fact that the S_0 magnitudes in the LWIR were larger than in the MidIR. The S_0 values in the LWIR were on the order of 10^{-3} W/cm^2-sr, while in the MidIR, they were on the order of 10^{-4} W/cm^2-sr. Notice that between 06:00 and 08:00, the S_0 for the grass and trees in both wavebands has a shorter lag time after the increase in air

temperature than the tank does. This is because the grass and leaves of the trees have low mass and, therefore, follow air temperature more rapidly than the tank. These details determine the temporal occurrence of thermal crossover periods between the tank and its background.

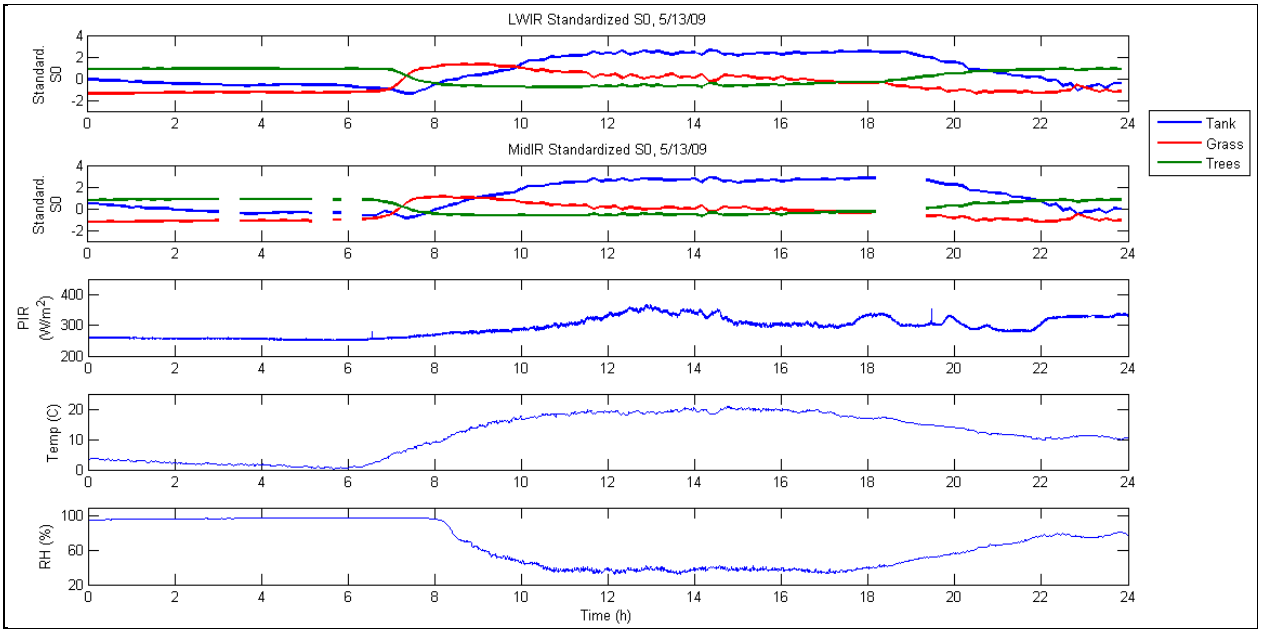

Figure 8. Diurnal plots of standardized S_0 values in the MidIR and LWIR for surrogate tank (blue), grass (red), and trees (green) regions of interest.

Figures 9 shows the MidIR and LWIR standardized diurnal plots of S_1 values for the test scene. The LWIR S_1 profiles for the grass and trees do not vary much, and the magnitude of the S_1 values for the tank is consistently larger than for the grass and trees. The S_1 values for the tank are negative which, given the geometry of the experimental setup, implies that the dominant component of the S_1 signature is due to emission. The variance in the S_1 curve for the tank is due to the presence of clouds that have moved into the area as the day progressed. The result is a decrease in the magnitude of S_1 for the tank. The clouds affect the scene in two ways: first, they decrease the amount of solar energy that reach the objects in the scene and, therefore, decrease the rate at which these objects are heated; and second, they act as additional sources of IR light because they radiate IR light as well as reflect the IR light emitted from the Earth back down onto the scene. This additional IR light is then reflected off of the more reflective objects in the scene (in this case, the tank) and becomes partially polarized (*8, 9*). This reflected component of polarization is oriented at 90° to and competes with the emitted component and effectively reduces the overall magnitude of the LWIR polarimetric signature of the tank.

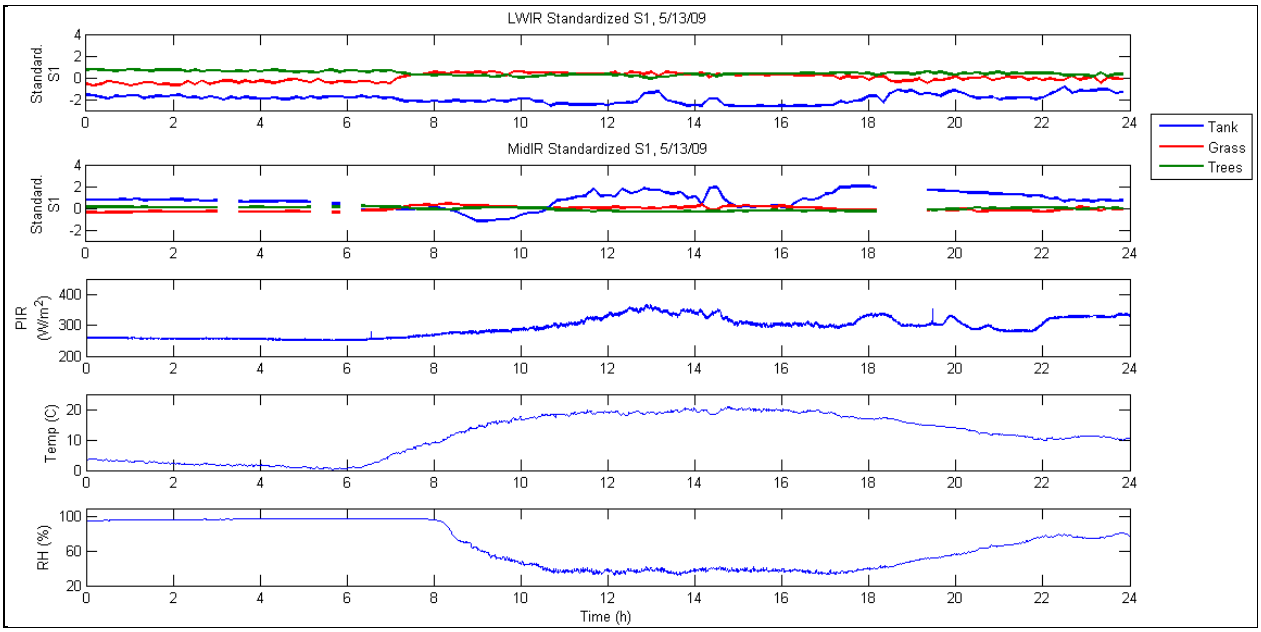

Figure 9. Diurnal plots of standardized S1 values in the MidIR and LWIR for surrogate tank (blue), grass (red), and trees (green) regions of interest.

Before sunrise, the MidIR S_1 signatures were very stable with the tank, having values slightly higher than the background. When the sun rose, the objects in the scene began to absorb photons and heat up. Between 06:00 and 09:00, this resulted in a crossover into an increasingly negative S_1 regime for the tank, suggesting that the dominant component of polarization is emission. After 09:00, this process reversed and the tank's MidIR S_1 signature experienced another crossover and remained positive for the remainder of the day. This positive S_1 magnitude was directly correlated with the presence of clouds in the sky. These observations are consistent with the clouds acting as a source of MidIR optical background that produced a reflected component greater than the emitted component (*10*).

3.2 Diurnal Contrast

Figures 10 and 11 show the diurnal contrasts between the tank and its natural background (grass and trees, respectively) in the LWIR S_0 and S_1 and MidIR S_1. The MidIR S_0 contrast is omitted because it is very similar to the contrast in the LWIR S_0. For the majority of the day, the contrast in LWIR S_1 is higher than in LWIR S_0 or MidIR S_1 and is reduced by the presence of clouds, which act as sources of LWIR optical background radiation. The peak in MidIR S_1 contrast between 08:00 and 10:00 is due to polarized emission resulting from the heating of the tank. As clouds begin to enter the atmosphere at 10:00, the tank's MidIR S_1 signature begins to acquire a larger reflective component, resulting in the crossover at approximately 10:30 and the subsequent contrast modulation throughout the rest of the day. The anti-correlation with the presence of clouds between the tank's LWIR and MidIR S_1 contrast is most readily observed between 12:00 and 16:00. Peaks in cloud cover at 13:00 and 14:30 are associated with decreases

in LWIR S_1 contrast and improvements in MidIR S_1 contrast, while during the period of relatively clear skies between 15:00 and 16:00, the LWIR S_1 contrast is at its maximum during the 24-h period and the MidIR S_1 contrast falls to zero.

The contrasts between the tank and the trees (figure 11) are similar to that between the tank and the grass with a few exceptions. The improved contrast between the tank and the trees in the LWIR S_1 was consistently greater during the periods 00:00 to 10:00 and 20:00 to 22:00 than between the tank and the grass. The two thermal crossovers between the tank and the trees occurred at 08:00 and 20:30. The MidIR S_1 contrast between the tank and trees is very similar to the case between the tank and the grass. Most importantly, the inverse correlation of the relationship of LWIR S_1 and MidIR S_1 to the presence of clouds remains between the tank and trees.

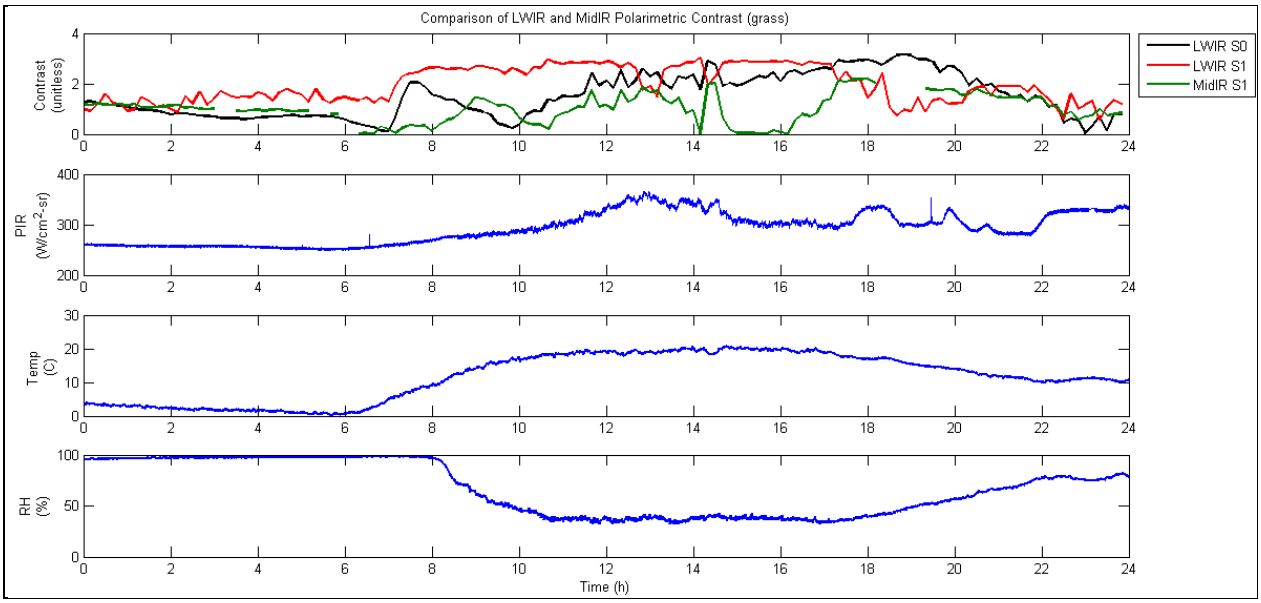

Figure 10. Diurnal contrast between the tank and its background of grass on May 13, 2009.

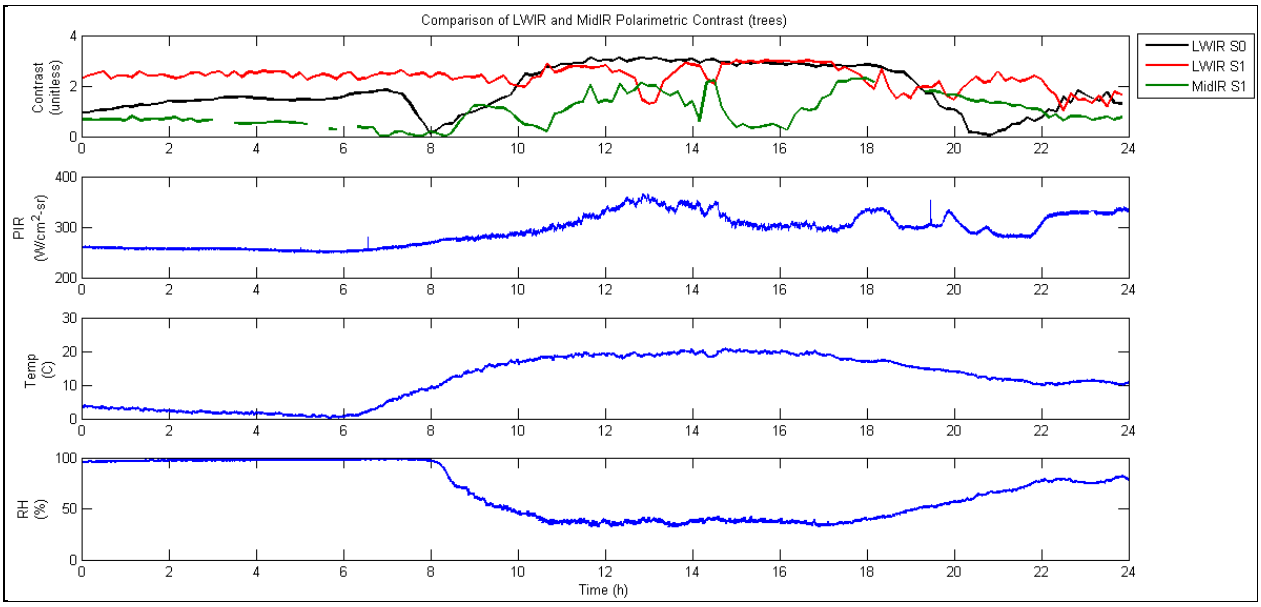

Figure 11. Diurnal contrast between the tank and its background of trees on May 13, 2009.

4. Conclusions

In this study, the temporal occurrence of conventional thermal and polarimetric inversions was examined, as well as their correlations to environmental factors. Imagery was recorded with two polarimetric IR sensors. The first was a LWIR sensor employing a 324×256 microbolometer array using a spinning achromatic retarder to perform the polarimetric filtering. The second was a MidIR polarimetric sensor based on a DOA approach with a 640×512 indium antimonide (InSb) FPA. The images used in this study included the S_0 and S_1 images of a scene containing a military vehicle and the natural background. In addition, relevant meteorological parameters measured during the test periods included air temperature, ambient loading in the LWIR, relative humidity, cloud cover, height, and density.

This study revealed that during most thermal inversion periods, a polarimetric contrast remained between at least some facet of the target—and in many cases, the whole target—and its background. In addition, the data showed that the chief factors affecting polarimetric contrast were the amount of thermal emission from the objects in the scene and the abundance of MidIR and LWIR sources in the optical background.

Furthermore, it was observed that the optical background due to cloud cover decreases LWIR S_1 contrast, while it increases MidIR S_1 contrast. This is consistent with the notion that MidIR polarimetric signatures tend to have a higher reflection component than LWIR polarimetric signatures.

Typical thermal inversions can affect contrast for up to 2 h at a time, reducing the effectiveness of thermal imaging systems and jeopardizing the success of military and security missions. The findings of this study suggest that conventional thermal imagery can be enhanced by incorporating fused MidIR and LWIR polarimetric information. The waveband that showed the most promise for polarimetrically enhancing conventional thermal imaging during this test was LWIR. The ability of LWIR polarimetric imaging to enhance conventional thermal imaging is limited by its susceptibility to the optical background. If a polarimetrically enhanced LWIR thermal imager is being used during a mission under conditions in which there are significant optical background sources, then the performance of the system will reduce to that of a conventional thermal system. By fusing LWIR and MidIR polarimetric data, it may be possible to extend the polarimetric enhancement of conventional thermal imagery into the periods of high optical background by exploiting the reflective nature of MidIR polarimetric signatures.

5. References

1. Shumaker, D. L.; Wood, J. T.; Thacker, C. R. *Infrared Imaging Systems Analysis*, DCS Corporation, Alexandria, VA, 1993, 2-45–2-49.

2. Tyo, J. S.; Goldstein, D. L.; Chenault, D. B.; Shaw, J. A. Review of Passive Imaging Polarimetry for Remote Sensing Applications. *App. Optics* **2006**, *45* (22), 5453–5469.

3. Tyo, J. S.; Ratliff, B. M.; Boger, J. K.; Black, W. T.; Bowers, D. L.; Fetrow, M. P. The Effects of Thermal Equilibrium and Contrast in LWIR Polarimetric Images. *Optics Exp.* **2007**, *15* (23), 15161–15167.

4. Pezzaniti, J. L.; Chenault, D. B. A Division of Aperture MWIR Imaging Polarimeter. *SPIE, 5888*, 239–245.

5. Pezzaniti, J. L.; Hyatt, B.; Reinhardt, J. Systems Users Manual: LWIR Rotating Retarder Imaging Polarimeter, 2008.

6. Dillon, W. R.; Goldstein, M. *Multivariate Analysis: Methods and Applications*; John Wiley & Sons: New York, Chichester, Brisbane, Toronto, and Singapore, 1984, pp 10–13.

7. Felton, M.; Gurton, K. P.; Ligon, D.; Raglin, A. *Discrimination of Objects Within Polarimetric Imagery Using Principle Component and Cluster Analysis*; ARL-TR-4216; U.S. Army Research Laboratory: Adelphi, MD, 2007.

8. Shaw, J. A.; Nugent, P. W.; Pust, N. J.; Thurairajah, B. Radiometric Cloud Imaging with an Uncooled Microbolometer Thermal Infrared Camera. *Optics Exp.* **2005**, *13* (15), 5807–5817.

9. Salby, M. L. *Fundamentals of Atmospheric Physics*; Academic Press: San Diego, New York, Boston, London, Sydney, Tokyo, and Toronto, 1996, pp 198–205.

10. Shaw, J. A. Degree of Linear Polarization in Spectral Radiances from Water-viewing Infrared Radiometers. *App. Optics* **1999**, *38* (15), 3157–3165.

List of Symbols, Abbreviations, and Acronyms

ARL	U.S. Army Research Laboratory
CO_2	carbon dioxide
DOA	division-of-aperture
FOV	field of view
FPA	focal plane array
H_2O	water
I^2	image intensification
InSb	indium antimonied
LWIR	long-wave IR
MidIR	mid-wave IR
PIR	precision infrared radiometer

No. of Copies	Organization
1 ELECT	ADMNSTR DEFNS TECHL INFO CTR ATTN DTIC OCP 8725 JOHN J KINGMAN RD STE 0944 FT BELVOIR VA 22060-6218
1 CD	OFC OF THE SECY OF DEFNS ATTN ODDRE (R&AT) THE PENTAGON WASHINGTON DC 20301-3080
1	US ARMY RSRCH DEV AND ENGRG CMND ARMAMENT RSRCH DEV & ENGRG CTR ARMAMENT ENGRG & TECHNLGY CTR ATTN AMSRD AAR AEF T J MATTS BLDG 305 ABERDEEN PROVING GROUND MD 21005-5001
1	PM TIMS, PROFILER (MMS-P) AN/TMQ-52 ATTN B GRIFFIES BUILDING 563 FT MONMOUTH NJ 07703
1	US ARMY ABERDEEN TEST CENTER ATTN TEDT AT WFT F CARLEN 400 COLLERAN ROAD ABERDEEN PROVING GROUND MD 21005-5009
1	US ARMY ARMAMENT RSRCH AND DEVELOPMENT ENGINEERING CTR ATTN AMSRD AAR MEF S L E ROTH BLDG 407 PICATINNY ARSENAL NJ 07806-5000
1	US ARMY CECOM RDEC NVESD ATTN AMSRD CER NV ST SIP J HOWE 10221 BURBECK RD STE 430 FT BELVOIR VA 22060-5806
1	US ARMY INFO SYS ENGRG CMND ATTN AMSEL IE TD A RIVERA FT HUACHUCA AZ 85613-5300

No. of Copies	Organization
1	COMMANDER US ARMY RDECOM ATTN AMSRD AMR W C MCCORKLE 5400 FOWLER RD REDSTONE ARSENAL AL 35898-5000
1	US ARMY RDECOM ARDEC ATTN M WOOLLEY BLDG 407 PICATINNY ARSENAL NJ 07806
1	US ARMY RDECOM ARDEC ATTN AMSRD AAR AEP S J ROMANO BLDG 407 PICATINNY ARSENAL NJ 07806-5000
1	US ARMY TARDEC ATTN AMSRD TAR MS 263 G GRANT 6501 EAST 11 MILE RD WARREN MI 48397-5000
1	AFRL/RYJT ATTN R T MACK 2241 AVIONICS CIRCLE BLDG 620 WRIGHT-PATTERSON AFB OH 45433-7320
1	AFRL/VS ATTN T R CAUDILL 3550 ABERDEEN AVE SE BLDG 423 KIRTLAND AFB NM 87117
1	AFRL/VSS ATTN M J DUGGIN 3550 ABERDEEN AVE SE KIRTLAND AFB NM 87117
1	USAFRL-VSSS ATTN M FETROW 3550 ABERDEEN SE KIRTLAND AFB NM 87117
1	US GOVERNMENT PRINT OFF DEPOSITORY RECEIVING SECTION ATTN MAIL STOP IDAD J TATE 732 NORTH CAPITOL ST NW WASHINGTON DC 20402

No. of Copies	Organization
1	JOHNS HOPKINS UNIVERSITY APPLIED PHYSICS LAB ATTN MP3-W110 A GOLDBERG 11100 JOHNS HOPKINS RD LAUREL MD 20723-6099
1	COLLEGE OF OPTICAL SCIENCES UNIVERSITY OF ARIZONA ATTN B M RATLIFF TUCSON AR 85721
1	UNIVERSITY OF ARIZONA COLLEGE OF OPTICAL SENSORS ATTN S TYO TUCSON AZ 85721
1	GEORGIA TECH RSRCH INSTITUTE ATTN J S ACCETTA 2015 YALE BLVD SE ALBUQUERQUE NM 87106
1	MONTANA STATE UNIVERSITY ATTN J SHAW 108 CULBERTSON HALL P.O. BOX 172000 BOZEMAN MT 59717-2000
2	POLARIS SENSOR TECHNOLOGIES INC ATTN D B CHENAULT ATTN J L PEZZANITI 200 WESTSIDE SQUARE STE 320 HUNTSVILLE AL 35801
1	US ARMY RSRCH LAB ATTN RDRL CIM G T LANDFRIED BLDG 4600 ABERDEEN PROVING GROUND MD 21005-5066
1	DIRECTOR US ARMY RSRCH LAB ATTN RDRL ROE V W D BACH PO BOX 12211 RESEARCH TRIANGLE PARK NC 27709

No. of Copies	Organization
15	US ARMY RSRCH LAB ATTN IMNE ALC HRR MAIL & RECORDS MGMT ATTN RDRL CIE S K GURTON (5 COPIES) ATTN RDRL CIE S M FELTON (5 COPIES) ATTN RDRL CIM L TECHL LIB ATTN RDRL CIM P TECHL PUB ATTN RDRL SEE E K KLETT, JR. ATTN RDRL SES E D ROSARIO ADELPHI MD 20783-1197

TOTAL: 41 (1 ELEC, 1 CD, 39 HCS)

INTENTIONALLY LEFT BLANK.